



Flinders

UNIVERSITY

Dynamical (e,2e) Studies of Bio-Molecules

Joseph Douglas Built-Williams

Submitted in fulfillment for the requirements
of the degree of Masters of Science

March 2013

School of Chemical and Physical Sciences
Flinders University of South Australia

If it's green or wriggles, it's biology.

If it stinks, it's chemistry.

If it doesn't work, it's physics.

~ Handy guide to Modern Science

3

Experimental Apparatus and Techniques

Throughout the project a variety of different experimental techniques were utilised. This chapter aims to provide a description of these techniques and also provide a general overview of the (e,2e) spectrometer that forms the basis of the measurements performed in this project.

3.1 Apparatus

3.1.1 Overview

The (e,2e) spectrometer is housed within a stainless steel vacuum chamber and functions by producing a monochromatic electron beam that interacts with a collimated molecular beam. Collisions takes place within a well defined volume known as the interaction region - a region which is shielded from electric fields by a grounded Faraday cage. If an ionising collision takes place, the resulting electrons are detected by two electrostatic hemispherical energy analysers upon which are mounted channel electron multipliers (CEMs). The two analysers are mounted on separate rotatable turntables and are configured in such a manner as to only allow electrons of a specific energy to pass through to the CEMs. By utilising fast timing electronics, the ionisation process may be characterised by correlating the angle at which the ejected electron was detected with the other kinematic variables in a process that is formally known as the (e,2e) coincidence technique. A labelled photograph of the present (e,2e) spectrometer can be seen in Figure 3.1. The following sections will go into greater detail about its specific components.

3.1. APPARATUS

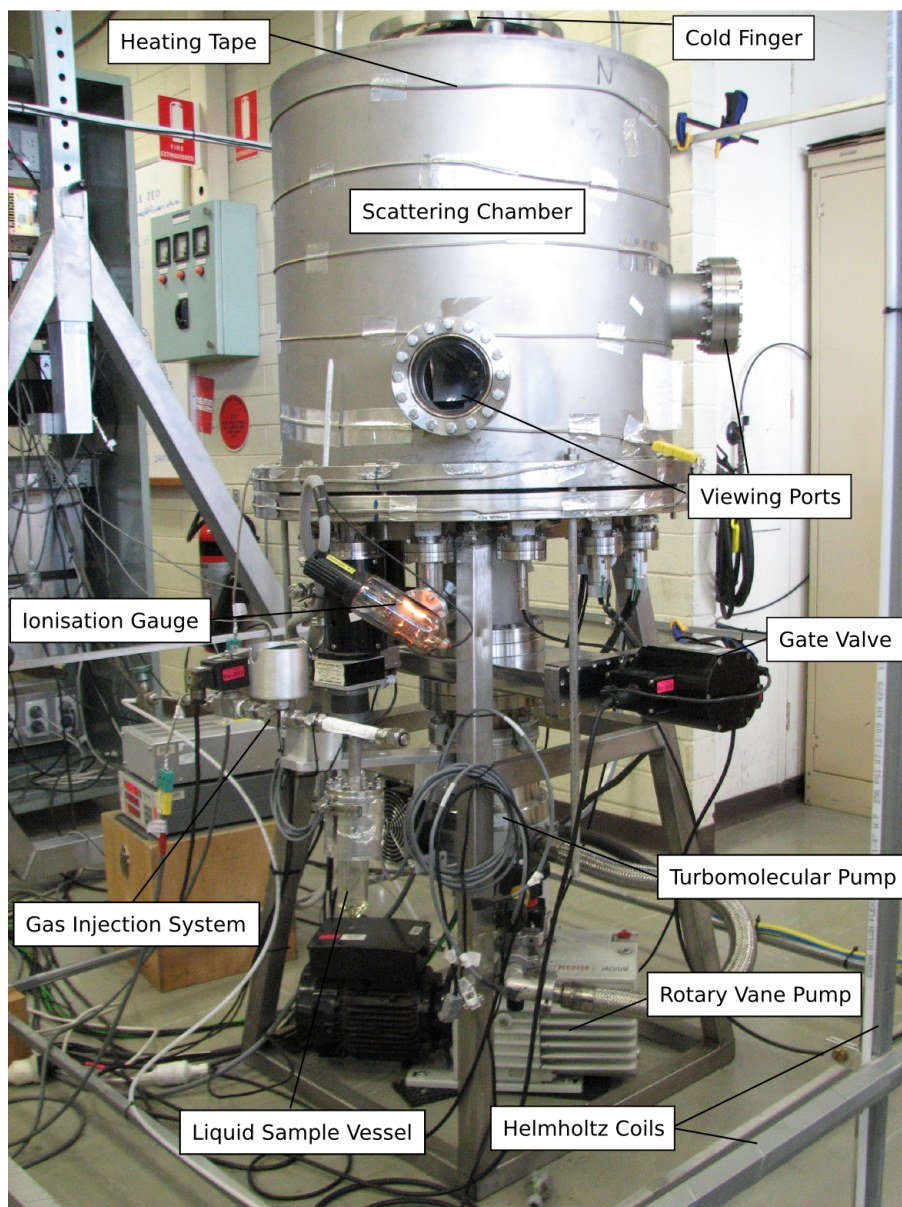


Figure 3.1: Exterior photograph of the present (e,2e) apparatus, illustrating its many external features as labelled.

3.1.2 Vacuum Chamber

The vacuum chamber of the current (e,2e) spectrometer (see Figure 3.2) consists of a chamber and a base plate, both of which are fabricated from type 310-stainless steel which has good non-magnetic properties. Within the chamber, an inner layer composed of 3mm thick μ -metal rests to eliminate or at least significantly reduce any external magnetic fields. The base plate of the vacuum chamber has twelve 2.75 inch Conflat flanges, that act as ports to which electrical and rotatable mechanical feedthroughs, leak valves for gas entry and pressure gauges are attached. In addition, two 3.75 inch viewing ports are positioned on the cylindrical chamber; one of which is located opposite the electron gun while the other is displaced 90° and is located opposite the gas capillary.

The chamber measures 600mm vertically and has an outer diameter of 614mm. A 6 inch Conflat port extends 95mm from the top of the chamber, while the two viewing ports extend 95mm out from its side. In addition, we note that the solid 310-stainless steel base plate has a diameter of 704mm and is 35mm thick.

During operation the chamber and base plate are warmed via heating tape, to ensure that the bio-molecules of interest don't contaminate the inner surface of the chamber as well as improving the speed in which the chamber may be degassed. To further reduce any molecular contamination, a 310-stainless steel cylinder is attached to the 6 inch Conflat port located on the top of the chamber such that it extends downward into the chamber. This acts as a 'cold finger' when it is filled with liquid nitrogen and provides a location on which bio-molecules can condense.

Of the twelve 2.75 inch Conflat flanges that are equally distributed around the circumference of the base plate, seven act as electronic feedthroughs for the (e,2e) spectrometer. Two others are used as mechanical feedthroughs for two stepper motors that are the motive force for the independent turntables. Another is solely used to admit the various target gases into the vacuum chamber. The final two Conflats have been employed to monitor the pressure of the vacuum chamber. Initially this was achieved with an ion gauge on one flange and a convectron gauge on the other. However, with the replacement of the ion gauge (see Chapters 4 and 6 for more details), the convectron gauge has become superfluous and has since been replaced with a blank Conflat flange.

The typical operating pressure of the vacuum chamber lies within the low 10^{-5} torr region, although base pressures down to 2×10^{-8} torr are not uncom-

3.1. APPARATUS

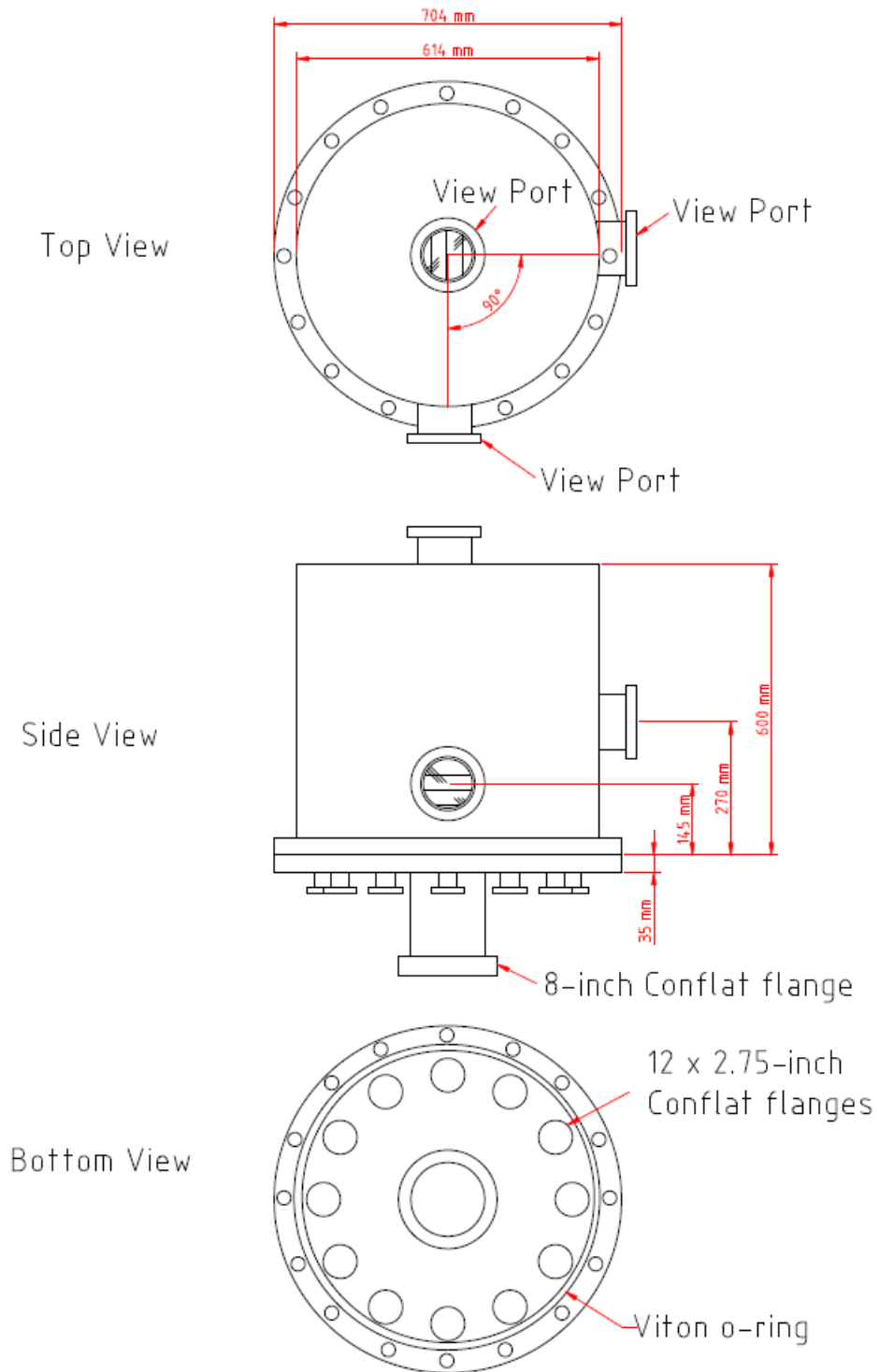


Figure 3.2: *The Flinders University (e,2e) spectrometer chamber schematic [9].*

CHAPTER 3. EXPERIMENTAL APPARATUS AND TECHNIQUES

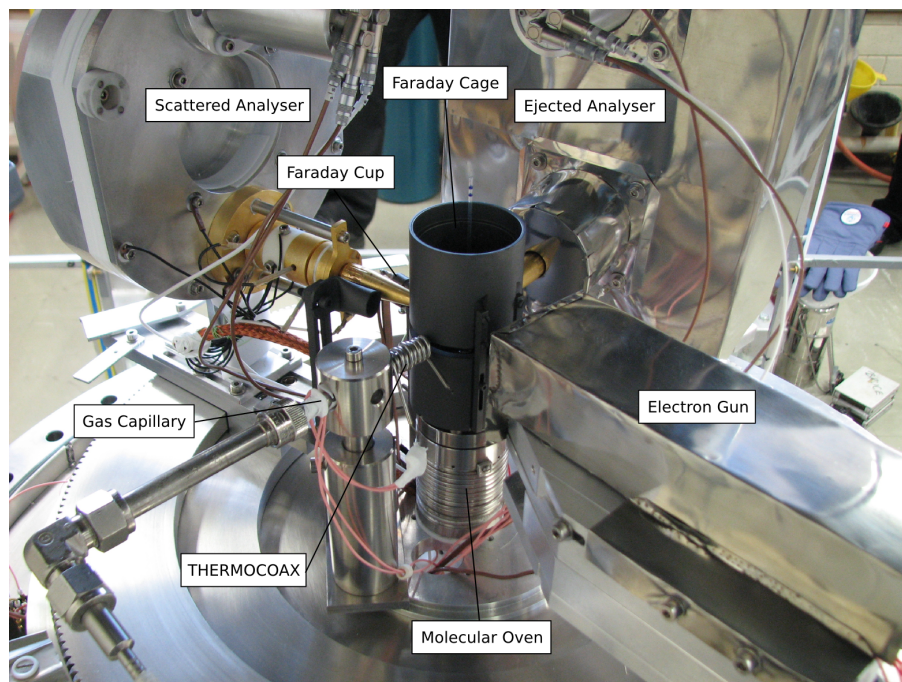


Figure 3.3: Photograph of the inside of the scattering chamber. Important elements of the spectrometer are as labelled.

mon when no sample is being introduced. This is achieved through the use of a Pfeiffer TMH 520 turbomolecular pump, which is connected to the base of the chamber by an electro-pneumatic gate valve and an 8 inch Conflat flange. A backing line runs via the turbomolecular pump to a Pfeiffer Duo 25 M rotary vane backing pump, the pressure in which is monitored by an additional convection gauge. Finally a seal is formed between the chamber and its base plate by a Viton o-ring.

Three sets of orthogonal 2.2m, square section, Helmholtz coil pairs surround the chamber, with the purpose of nullifying external magnetic fields. This is in addition to the aforementioned layer of μ -metal that lines the chamber. We note that the two systems working in conjunction can reduce the magnetic fields within the chamber below the 2mGauss mark. Within the vacuum chamber, a grounded Faraday cage surrounds the interaction region to nullify any stray electric fields that could distort the paths of the incident, scattered and ejected electron beams. This feature can clearly be seen in Figure 3.3.

Mounted on the base, and within the vacuum chamber, is a stainless steel plate of diameter 440mm and thickness 10mm. Two independently rotatable turntables rest upon this plate, separated by v-shaped channels containing 4mm diameter ceramic spheres. These spheres are evenly distributed through the use

of stainless steel races. This allows the turntables to rotate smoothly in the scattering plane. Additionally, the two turntables are geared to the mechanical feedthroughs which are in turn connected to computer-controlled steppermotors.

Outside of the Helmholtz coils there is a simple frame attached to a 1 ton pulley, which allows for the easy removal of the vacuum chamber lid. While the system is in operation, the pulley and attached chain, may be moved outside of the Helmholtz coils to minimise any magnetic field interference that they might cause. Finally, the vacuum chamber is raised 950mm off of the laboratory floor, by a simple four legged frame, providing the space necessary for the turbomolecular and backing pumps to rest beneath it.

3.1.3 Electron Gun

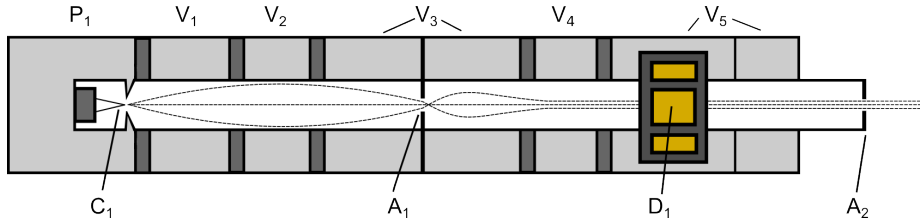


Figure 3.4: *Schematic diagram of the electron gun used in the present measurements.*

The electron gun in the (e,2e) spectrometer is of a typical design, utilising a cathode (C_1), a series of electrostatic lenses ($V_1 - V_5$), collimation apertures (A_1, A_2) and a single set of deflectors (D_1). This design allows for the creation of a collimated electron beam, an example of which can be seen in Figure 3.4. As the electron gun has been described in great detail elsewhere [15, 9], only a brief overview will now be given.

The electron source is a simple tungsten filament mounted on a ceramic base, located at C_1 in the above figure. This filament is known as a ‘needlepoint’ type filament, due to its particular ‘V’ shape. This configuration is used as it reduces the emitting area of the filament to a well defined point. Electrons are initially emitted from the filament when a current of $\sim 1.15\text{A}$ is applied, however it is typically common to have between $1.3\text{A} - 1.4\text{A}$ applied through the filament to ensure a stable electron beam of sufficient flux for the (e,2e) measurements is achieved.

Surrounding the tungsten filament is the ‘Pierce’ element, P_1 , which forms an enclosing cylinder with a single 1mm hole in one end, precisely centred over the needlepoint of the filament. The Pierce electrode acts as an initial focusing element for the electron beam. By applying a negative potential across the Pierce

CHAPTER 3. EXPERIMENTAL APPARATUS AND TECHNIQUES

element, the angular spread of the electrons leaving the filament is reduced, encouraging more electrons to exit through its aperture. A thin Macor ring is located between the Pierce element and V_1 , as well as between all the subsequent electron gun lens elements. These act as spacers to ensure the separation of the respective lens elements.

V_1 , V_2 , V_3 , V_4 and V_5 are 310-stainless steel cylindrical lens elements to which a potential is applied. The difference between these potentials sets up electrostatic fields that influence the path of the electrons, acting much like optical lenses. Like optical lenses, these electrostatic lenses focus the divergent electrons with the end result being a highly collimated electron beam following a largely parallel path with respect to the axis of symmetry of the electron gun. A great deal of control can be exerted over the electron beam by varying the potentials between successive elements. In general, this follows the electrostatic equivalent of Snell's Law [80]:

$$\sqrt{V_1} \sin \alpha_1 = \sqrt{V_2} \sin \alpha_2, \quad (3.1)$$

where $V_{1,2}$ are the voltages applied to the lens(es) and $\alpha_{1,2}$ is the deflection experienced by the electron, with respect to the normal formed by the path of the charged particle in the two regions of differing electrostatic potential. This equation, known as the Helmholtz-Lagrange law, applies for all the lens elements in the electron gun. A typical path of the electrons through the electron gun, for values of $V_1 - V_5$ we often employ, can be seen in Figure 3.4, appearing as dotted lines, and are representative of the true electron path which was determined using the SIMION charged-particle optics code [81].

Furthermore, two apertures are located at A_1 and A_2 , arranged in the middle of V_3 and at the end of the electron gun respectively. These apertures bear a 1mm hole in their centre and are formed of 310-stainless steel, again because of that materials non-magnetic properties. As can be expected, the purpose of these apertures is to remove electrons following an aberrant path, thus improving the collimation of the electron beam.

Finally D_1 , located within V_5 , is a deflector array: a system of four solid 310-stainless steel wedges. This array allows for some level of control over the horizontal and vertical position of the collimated electron beam within the interaction region.

The complete electron gun is mounted upon a 310-stainless steel base set at

what is defined as the 180° mark, as can be seen in Figure 3.3. A thin Advance metal cover protects the electron gun from any stray electric fields, as well as shielding the rest of the (e,2e) spectrometer components from the potentials of the lens elements. In addition a thin graphite film covers the Faraday cage surrounding the interaction region, which reduces stray electrons from the electron gun scattering in random directions due to its good electrical conductivity.

All the electrostatic lenses (including the Pierce element), except V_5 , are floated relative to the electron beam energy, with V_5 being grounded. The four individual lenses ($V_1 - V_4$) have a voltage applied to them, relative to the float, by four separate power supplies capable of supplying up to 1000V for each of the lenses. The Pierce element also has its own supply, capable of supplying it with up to $\pm 50V$, with 10mV precision. Finally the two deflector pairs (horizontal and vertical) each have a separate $\pm 15V$ power supply and are biased on the V_5 lens supply.

3.1.4 Analysers

Within the vacuum chamber, two hemispherical electron analysers are mounted on independently rotatable turntables, driven by two stepper motors. These analysers are traditionally known as the scattered and ejected electron analysers, named primarily for the fast and slow electrons, respectively, that results from the ionisation process. These electrons play an integral role in terms of the fast timing electronics (see Section 3.1.6 for more details), with the ‘start’ pulse being supplied by the scattered electron analyser while the ‘stop’ pulse is provided by the ejected electron analyser.

Due to the presence of the electron gun, as well as the gas capillary (see Section 3.1.3 and 3.1.5 respectively), both analysers are only able to move over the -50° to 120° angular range in the scattering plane. This is further impeded by the physical size and shape of the analysers, which limits them to coming no closer than within approximately 30° of one another. See Figure 3.6 for details.

The analysers are made up of three parts: a focusing array, two hemispheres, and a detector. The first part is quite similar to the electron gun discussed in Section 3.1.3. Like the electron gun, the focusing array is made up of a series of cylindrical electrostatic lenses (V_1, V_2, V_3, V_4 and V_5 on Figure 3.5), apertures (A_1 and A_2) and a set of deflectors (D_1). Unlike the electron gun, however, the focusing array elements are separated by a number of sapphire balls.

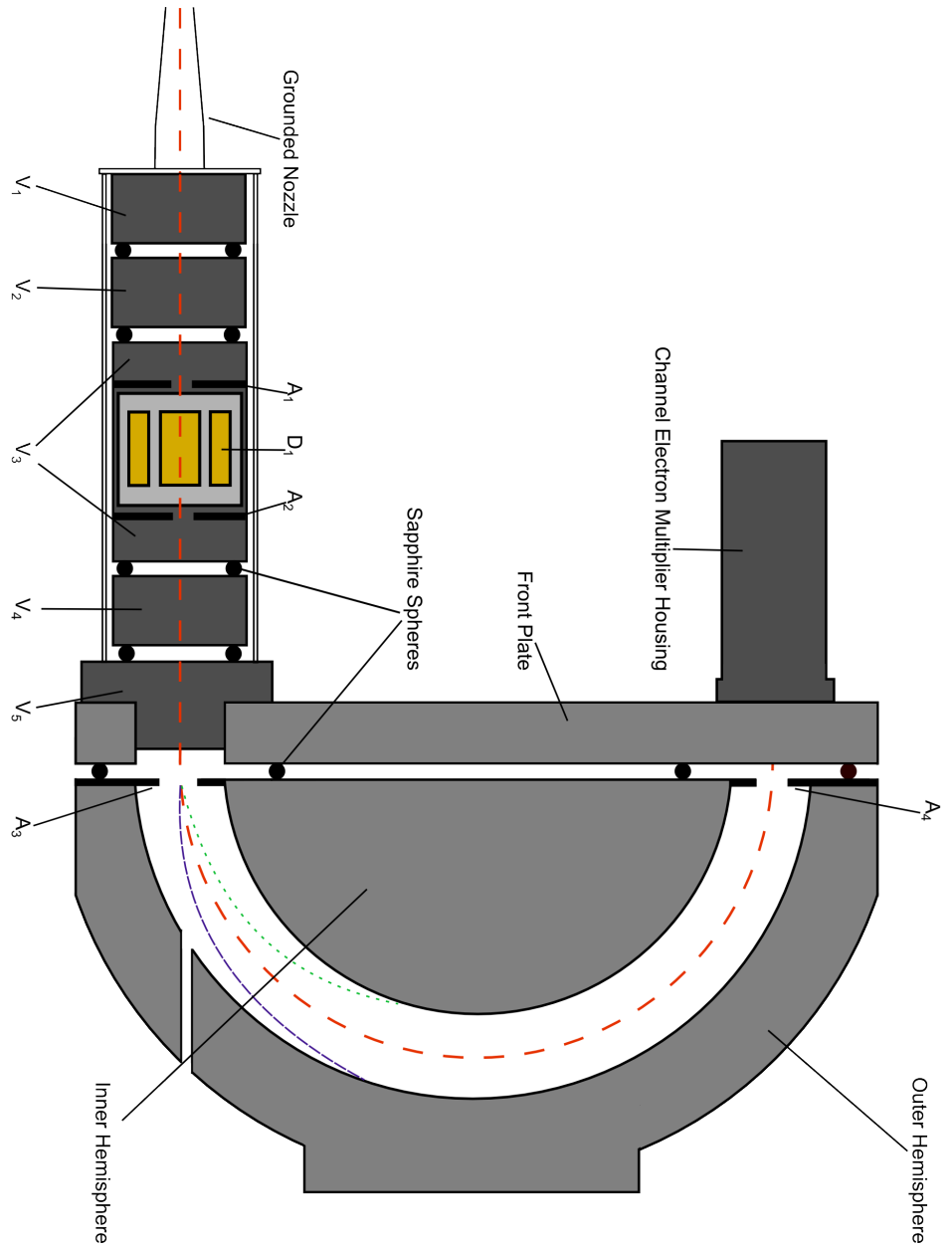


Figure 3.5: Schematic diagram of an analyzer. The red line traces out the path that electrons of $E_p = eV_p$ take, the green dotted line traces out a possible path for electrons of energies $E > E_p$, while the blue dashed line traces out a possible path for the electrons of energies $E < E_p$. Insulation between the various elements is provided by 1 mm sapphire balls.

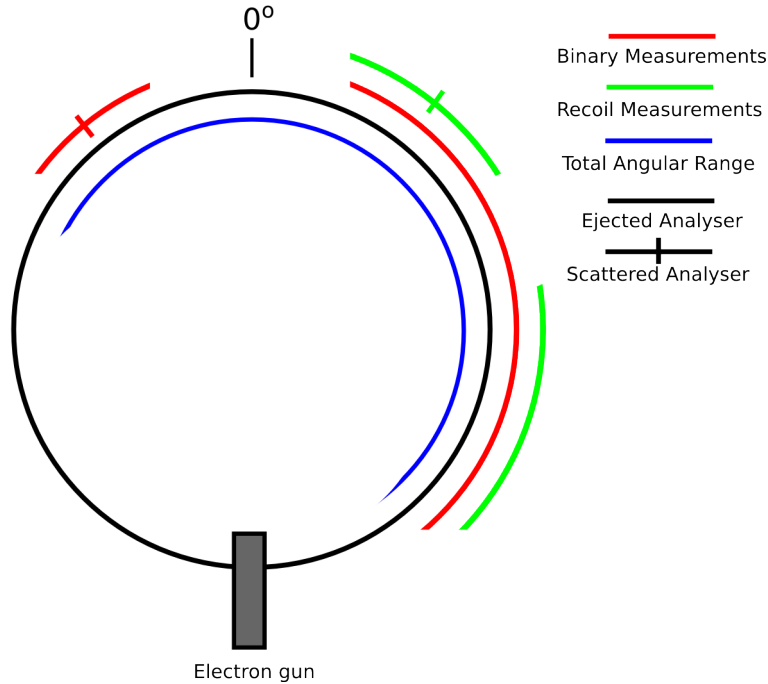


Figure 3.6: A schematic diagram of the scattering region, as seen from above, highlighting the manner in which binary and recoil measurements are taken given the limited angular range.

In the present case the focusing array electrostatic lenses are formed from oxygen-free high conductivity copper and plated with a $1 \mu\text{m}$ thick layer of gold, which was added to provide a measure of corrosion resistance and to further improve conductivity. The electrostatic lens V_1 is grounded, while the lenses V_2 , V_3 , V_4 and V_5 are referenced first to the pass energy of the hemisphere, V_p , which in turn is floated on a reference voltage which is set at the specific scattered or ejected electron energy being studied.

The deflectors of the focusing array, D_1 , are located within the electrostatic lens V_3 , and sandwiched between the two apertures A_1 and A_2 . Much like the deflectors of the electron gun, this set of deflectors is made up of four quarter annuli, although now they are fabricated from oxygen-free high conductivity copper. The purpose of the deflectors in the focusing array is to compensate for any minor misalignment of the focusing array.

The hemispheres of the analysers are made from ultra-high vacuum compatible aluminium, the inner surface (defined as the surface that “sees” the electrons) of which is coated with a $1 \mu\text{m}$ layer of gold, to minimise surface charging. Both hemispheres are kept electrically isolated from the front plate of the analyser, and each other, by a combination of 4mm sapphire spheres and ceramic and

CHAPTER 3. EXPERIMENTAL APPARATUS AND TECHNIQUES

Teflon insulators. Two 2mm apertures (A_3 and A_4) are located at the ‘entrance’ and ‘exit’ of the hemispheres respectively: the purpose of which is to limit any aberrant electrons from accessing the detector. A 1mm hole is also present in the outer hemisphere, that is in line with the central axis of the focusing array. This hole exists entirely for the purpose of aligning the analysers with respect to the interaction region, and has little to no effect upon their performance [82].

The electrostatic field generated by the potential difference between the two hemispheres deflects the electrons in a circular path, the radius of which is directly dependant upon the energy of the electrons [83, 84]. By varying the potential difference between the two hemispheres, one can effectively isolate electrons of a specific energy, known as the pass energy (E_p). An electron of pass energy $E_p = eV_p$ will trace out a circular path of radius r_p , which is at the mean radius of both the inner and outer hemispheres [83, 85] (see Figure 3.5). Electrons with an energy greater than the pass energy (i.e. $E > E_p$) will undergo lesser deflection, while electrons with an energy smaller than the pass energy (i.e. $E < E_p$) will undergo a greater level of deflection. In either case, the electron will be deflected into either of the hemispheres or aperture A_4 [86]. These alternative paths are presented in Figure 3.5 by the dotted and dashed lines shown there.

To calculate the required potentials that must be applied to the inner hemisphere, V_i , and the outer hemisphere, V_o , in order for an electron, of pass energy $E = eV_p$, to achieve the desired outcome, one must use the following equation for the inner hemisphere:

$$V_i = V_p \left(2 \frac{r_p}{r_i} - 1 \right) \quad (3.2)$$

and for the outer hemisphere:

$$V_o = V_p \left(2 \frac{r_p}{r_o} - 1 \right), \quad (3.3)$$

where $r_i = 50\text{mm}$ and is the radius of the inner hemisphere; $r_o = 75\text{mm}$ and is the radius of the outer hemisphere; and $r_p = \frac{r_i + r_o}{2} = 62.5\text{mm}$ is the mean radius, as well as being the radius of the path followed by the pass energy electrons. The origin of these equations can be found in reference [82].

In general, the energy resolution of a hemispherical analyser is given by [87]:

$$\frac{\Delta E}{E} = \frac{\omega}{r_p(1 - \cos \phi) + l \sin \phi}, \quad (3.4)$$

3.1. APPARATUS

where $\omega = 2\text{mm}$ and is the width of the entrance and exit apertures, l is the distance between the exit boundary of the analyser and the exit aperture, and $\phi = 180^\circ$ and is the spherical deflection of the analyser. Due to the fact that $\phi = 180^\circ$, Equation 3.4 can be simplified to:

$$\Delta E = \frac{E\omega}{2r_p}. \quad (3.5)$$

Thus, from looking at Equation 3.5, it should be clear that the only variable is the pass energy E , and so in order to adjust the energy resolution of this particular apparatus one must merely change E or the variable it depends on, V_p .

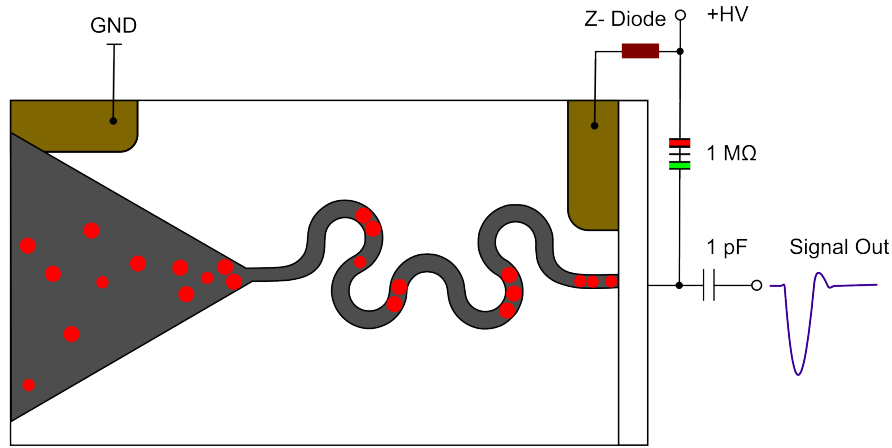


Figure 3.7: Schematic diagram of a Channel Electron Multiplier and signal ‘pick-off’ circuitry.

After the electron exits the hemispheres, it is detected by a Sjuts KBL5RS Channel Electron Multiplier (CEM). The CEM is mounted behind A_4 and is isolated in a cylindrical aluminium casing, complete with high voltage Lemo connectors and a cone at the entrance to the CEM. The CEM receives the electrons that have the required pass energy, and outputs a small pulse which acts as an input for the fast timing electronics (see Section 3.1.6). A schematic diagram of the CEM can be seen in Figure 3.7.

The CEM works on the same principle as a Geiger counter - when a single ionising particle (specifically an electron) strikes the surface of the CEM, a cascade of secondary electrons is created. When this cascade reaches the anode of the CEM, a noticeable negative pulse is produced [88].

This cascade is achieved in the CEM by applying a large potential (between

CHAPTER 3. EXPERIMENTAL APPARATUS AND TECHNIQUES

1.5 keV and 3.5 keV depending on the age of the CEM) over its highly resistive surface. This causes the formation of a continuous dynode that, when under the influence of an ionising particle, ejects secondary electrons [88]. The large potential continues to accelerate the primary and now secondary electrons through the CEM and, in turn, the electrons continue to interact with the CEM surface causing tertiary, etc, electrons to be ejected. Thus, from an initial electron, $\sim 1 \times 10^8$ electrons reach the anode at the end of the CEM tube, causing the production of a single pulse with a Full Width Half Maximum (FWHM) of approximately 8 nanoseconds.

3.1.5 Molecular Beam Source

The target gas enters the interaction region via a 316-stainless steel capillary located at the -90° location. The capillary can be mounted both perpendicular and in plane with the electron gun, is 50mm in length and has an inner diameter of 0.69mm. A nylon tube connects the capillary to one of the access ports in base of the vacuum chamber, which in turn is connected to a leak valve. The leak valve is connected via a t-junction to either a 1,000mbar gas reservoir or a glass sample vessel. An overview of this arrangement can be seen in Figures 3.1 and 3.3.

The 1,000mbar gas reservoir is a simple stainless steel vessel that usually holds high purity argon or helium, which are used for calibration purposes (see Section 3.3). Two valves and a number of meters of nylon tubing separate the gas reservoir from the common t-junction and the leak valve into the vacuum chamber. Furthermore the gas reservoir may be individually pumped out through the use of a JVAC DD300 vacuum pump, and can be isolated from the rest of the system by a 3-way valve. This latter facility also allows us to refill the reservoir with the gas of choice.

Volatile biomolecular targets are stored and prepared within the glass sample vessel, which is separated from the common t-junction and leak valve by another valve and a solenoid. That solenoid is in particular noteworthy as it will automatically shut in the event of a system failure, isolating the target sample from the vacuum chamber.

During the experiment, most of the biomolecular targets used had rather low volatility at room temperature. That volatility was improved upon by subtly heating the glass vessel. In addition, by heating the gas lines leading into the vacuum chamber, and the leak valve, condensation occurring within the gas

lines is averted. Furthermore, the stainless steel capillary is heated through the addition of a THERMOCOAX twin core heating element that has been wrapped around it. The THERMOCOAX was specifically chosen for its negligible magnetic field contributions.

In addition to the gas and liquid handling system, the Flinders (e,2e) spectrometer is outfitted with a molecular oven capable of safely vapourising solid-state biomolecules. Centred in the chamber, and resting beneath the interaction region, the cylindrical molecular oven is constructed from non-magnetic 310-stainless steel. The oven body has an outer height of 51mm, an inside height 37mm, an outside radius of 22.5mm and an inner radius of 15.5mm, providing a sum total of 27cm³ of volume in which a sample may be placed. A short capillary mounted on the oven lid forms the only egress from the molecular oven and extends a further 51mm above the oven body.

The oven and the lid can be independently heated by THERMOCOAX twin core heating elements, that are wound about the oven and lid in specially cut 1.5mm grooves. The temperature of the oven and needle can also be individually measured via K-type thermocouples. While the oven was not used for the duration covered by this thesis, the convenient location of its associated needle allows for easy visual calibration of the two analysers and the electron gun.

3.1.6 Racks

The racks contain a number of important control and analysis systems for the present (e,2e) spectrometer. As can be seen in Figure 3.8, the control systems are mostly self-explanatory and as many of the components are standard and have been explained many times previously [15, 9], we provide only a brief description here in preference of explaining some of the more complicated systems encapsulated by the racks.

The fast timing diagnostics represent some of the more important aspects of the racks, and perform the task of processing the raw signals from the CEMs into a more useful form. After an electron has been detected within a CEM, and a negative signal pulse generated by an electron cascade, the signal is passed through an Ortec 9301 pre-amplifier which is mounted immediately outside the chamber. This boosts the signal amplitude by a factor of 10 before the signal is fed into a quad Constant Fraction Discriminator (CFD).

The Ortec 934 QUAD CFD is a Nuclear Instrumentation Module (NIM) that

CHAPTER 3. EXPERIMENTAL APPARATUS AND TECHNIQUES



Figure 3.8: Photograph of the control racks, with the various important elements labelled as appropriate.

contains four independent CFDs, two of which accept the amplified negative pulse from the CEMs to generate two simultaneous fast negative logic pulses with constant rise times and amplitudes. One of the pulses, the one originating from the scattered analyser, acts as a start pulse for a Time-to-Amplitude Converter (TAC) NIM while the other pulse, originating from the ejected analyser, is delayed, via a delay line, by 62ns and acts as a stop pulse. The TAC is used to measure the time interval between the start and stop pulses and produces an analogue output pulse proportional to that measured time difference.

3.1. APPARATUS

The output of the TAC is then sent to a computer via a shielded National Instruments BNC-2120 connector block and a National Instruments high speed data acquisition PCI-6251 card. This allows for custom made LabView 8.5 scripts to perform further processing and analysis.

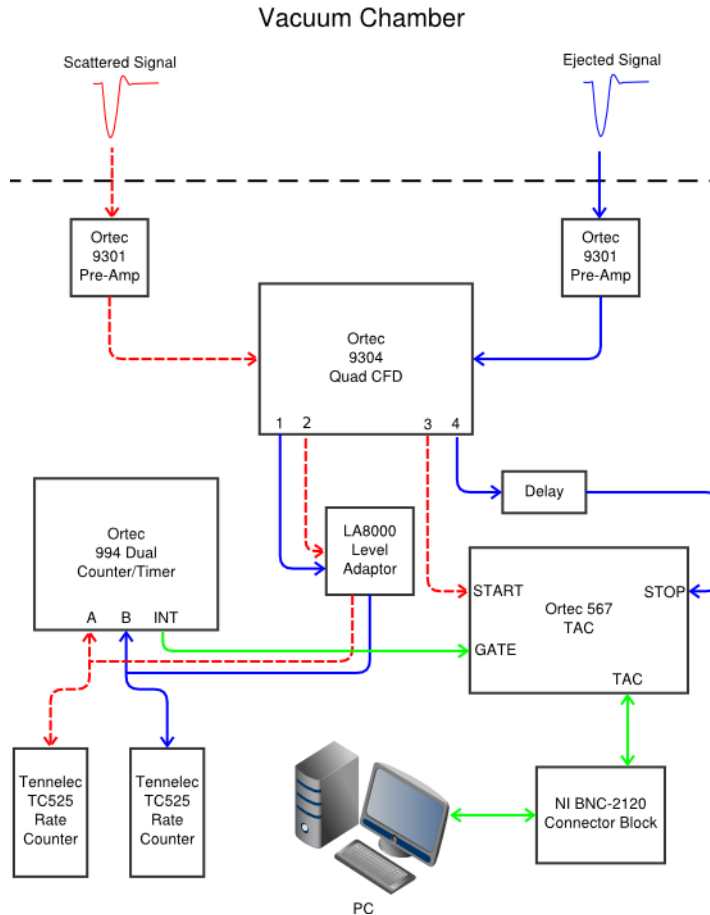


Figure 3.9: Flowchart of the operational aspects of the control racks. The red dashed line follows the path of a signal from the scattered analyser, while the blue solid line follows that of the ejected analyser.

In addition, the original amplified signals from the CEMs are, in fact, output twice by the Ortec QUAD CFD. The second set of signals are passed through a LA8000 level adaptor, the purpose of which is to convert the signals from the NIM into the TTL pulses so that they may be used with a counter and two ratemeters. The two Tennelec ratemeters, one for the scattered and one for the ejected electron analyser, are used to monitor the experiment as well as for tuning purposes.

The Ortec 994 dual counter/timer is used to count the number of scattered

CHAPTER 3. EXPERIMENTAL APPARATUS AND TECHNIQUES

electrons detected by the detector to a predetermined preset, the purpose being to make the collection of data independent of any incident electron beam and gas pressure variations. Furthermore, the counter/timer acts as a gate to the TAC so that when the preset is reached the collection of data is effectively stopped. A complete overview of the entire process, from electron detection until processing and analysis with the computer, can be seen in Figure 3.9.

3.2 Experimental Techniques

3.2.1 Coincidence Method

The coincidence method is an essential technique as it allows for the differentiation between electrons emanating from a specific ionisation event and ‘random’ or background electrons. This is achieved by measuring the temporal correlation between the outgoing electrons, and determining which electrons are from a specific ionisation event and which are random. As alluded to in Section 3.1.6, the temporal correlation is measured by the TAC: the time difference between the fast scattered electron and the slower ejected electron is converted into a proportionally sized analogue signal.

However, the time between the arrival of the scattered and ejected electrons is very small due to the high velocity of the electrons. A time delay of 62ns is thus introduced into the fast-timing electronics in order to counter this problem, and move any coincidence peak away from the leading edge of the timing spectrum (see Figure 3.10). This signal is then interpreted by the computer and plotted. If multiple electrons emanate from a specific ionisation event, then there will be a correlation in the outgoing electron times, producing a narrow ‘coincidence’ peak. The electron-pair counts that form the coincidence peak are known as ‘true coincidence counts’ while all other electron-pairs are known as ‘random coincidence counts’.

Figure 3.10 shows a typical timing spectrum, with all of the major features labelled. Of particular note is the fact that the timing spectrum is broken up into three “windows”. The range in which the coincidence peak forms is known as the signal window and has a width of Δt_c , which, in the present experimental configuration, is 10ns in width. The rest of the timing spectrum is known as the background window, and is made up of random coincidence counts. The width of the background window is $\Delta t_b = \Delta t_{b1} + \Delta t_{b2} = 470$ ns in the current experimental configuration. On either side of these three windows is a 5ns buffer of counts which are not included, leading to a total of 500ns being covered by the timing spectrum.

It should be noted here that if the energy of the scattered and ejected electrons approach one another in magnitude, the signal window will move along the horizontal axis and approach the origin. If such an occurrence happens, the 62ns delay can be increased, moving the signal window back to a more convenient position. Another point of note is the finite size of the signal window; in a perfect

CHAPTER 3. EXPERIMENTAL APPARATUS AND TECHNIQUES

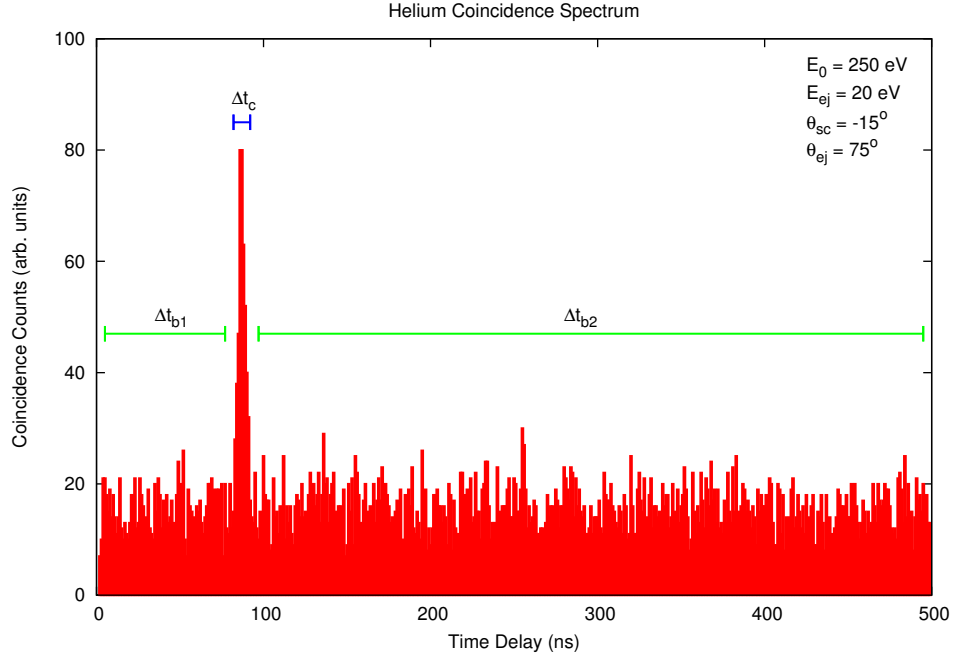


Figure 3.10: A typical timing spectrum of helium, with the signal window ($\Delta t_c = 10$ ns, blue), containing the coincidence peak, and background windows ($\Delta t_{b1} = 72$ ns and $\Delta t_{b2} = 398$ ns, green) as labelled. Note: there is a 5 ns buffer between the signal window, background windows and the ‘edges’ (i.e. at $t = 0$ and 500 ns).

world, Δt_c would approach 1ns in size, as all the electron-pairs originating from the same ionisation process should have a constant temporal coincidence rate [69]. The dispersion of the arrival times of the scattered and ejected electrons, in Δt_c , can be attributed to a combination of three experimental factors [69]:

- i) The interaction region size: ionisation events can occur at different points within the bounded interaction region. This leads to a small but perceptible variation in the path length of the electrons and thus a variation in arrival times, culminating in a slight broadening of the coincidence peak in the timing spectrum [89].
- ii) The kinetic energy of the electrons: The incoming electrons do not all share precisely the same kinetic energy. While electrons that possess kinetic energy that is vastly different to the pass energy, E_p , of the analysers will fail to reach the detectors, the electrons that only slightly differ from E_p can make it through to the CEM. This is due to the finite size of the apertures in the analysers, and in particular Aperture A_4 . This also leads to a slight variation in the time of flight of the electrons and thus a broadening of the coincidence peak in the timing spectrum [89].
- iii) Electronic jitter: As a part of the fast-timing electronics, the discriminator serves the purpose of reducing noise within the measurements. The

3.2. EXPERIMENTAL TECHNIQUES

discriminator does so by triggering only when the signal is larger than a minimum threshold voltage. However the variations in the amplitude of the signals causes the discriminator to trigger at different times [15].

The total number of true coincidence counts, N_t , can be determined by subtracting the total number of random coincidence counts, N_r , from the total number of coincidence counts that occur within the signal window, N_c . This is not as straight-forward as it seems, as the true value of N_r can only be inferred from the number of counts that occur within the background window, N_b . Thus:

$$\begin{aligned} N_t &= N_c - N_r \\ &= N_c - \frac{N_b}{r}, \end{aligned} \tag{3.6}$$

where;

$$r = \frac{\Delta t_b}{\Delta t_c}. \tag{3.7}$$

However, Equation 3.6 is based upon the assumption that the random counts are uniformly spread across the background windows Δt_{b1} and Δt_{b2} . This is not necessarily the case, and so other functions are required to determine the number of random coincidence counts in the signal window.

Thus it is necessary to know the standard deviation of the number of true coincidence counts, given by [73]:

$$\begin{aligned} \sigma_t &= \sqrt{N_c + \frac{N_b}{r^2}} \\ &= \sqrt{N_c + \frac{N_r}{r}}. \end{aligned} \tag{3.8}$$

It is clear from Equation 3.8 that in order to improve the standard deviation, σ_t , the ratio between the background and signal windows, r , should be as large as possible (see Equation 3.7). Thus it is desirable to ensure the background window, Δt_b , is as large as possible relative to the signal window, Δt_c . However, the ratio r must be accurately known, otherwise a systematic error will arise in the calculated value of N_t ; especially if $N_t \ll N_r$. It is also advisable to have the ratio r in the order of 10, as this will reduce statistical errors [73].

The limitations and advantages of the coincidence technique can be determined

CHAPTER 3. EXPERIMENTAL APPARATUS AND TECHNIQUES

from the true coincidence counts and the associated statistical uncertainty. As such, it becomes necessary to define the true coincidence count rate, R_t , in terms of the experimental parameters [73]:

$$R_t = nI\sigma^5 \Delta E_a \Delta E_b \Delta \Omega_a \Delta \Omega_b \delta(E_0 - E_a - E_b - \epsilon_i), \quad (3.9)$$

where σ^5 is the electron impact ionisation TDCS (see Equation 2.7), n is the target density, I is the incident electron beam current and ΔE_a , ΔE_b , $\Delta \Omega_a$ and $\Delta \Omega_b$ are instrumental parameters that determine the resolution of the experiment and represent the energy and angular resolution respectively.

The number of random coincidence counts, R_r , within the signal window, Δt_c , is given by the product of the singles electron count rates measured in each analyser, R_a and R_b , and the width of the signal window. *Id est*:

$$R_r = R_a R_b \Delta t_c. \quad (3.10)$$

For the individual analysers, the singles count rate is given by;

$$R_a = nI \frac{\sigma^2}{d\Omega_a dE_a} \Delta \Omega_a \Delta E_a \quad (3.11)$$

and

$$R_b = nI \frac{\sigma^2}{d\Omega_b dE_b} \Delta \Omega_b \Delta E_b, \quad (3.12)$$

where $\frac{\sigma^2}{d\Omega_n dE_n}|_{n=a,b}$ is the double differential cross section per unit solid angle and energy for an outgoing electron in the direction θ_a with energy E_a (see Section 2.3.2).

It can be seen from Equations 3.10, 3.11 and 3.12 that R_r is dependant upon R_a and R_b and any reduction that occurs in either will likewise lead to a reduction in R_r . Meanwhile, R_a and R_b are dependent on the singles counts that arrive in each detector. This it is clear that R_r is dependent upon the singles counts detected, and so it is important to reduce the unrelated/background counts measured by each detector.

This can be achieved in a number of different ways, with some of these having previously been mentioned in Section 3.1.2. Other implemented methods include coating the surfaces around the analysers, and particularly in the interaction region, with a thin graphite film, as well as introducing simple Faraday Cup-like “beam-dumps” either side of the scattered analyser (see Figure 3.3 for details). It should also be noted that the idea that Δt_c should be minimised is

3.2. EXPERIMENTAL TECHNIQUES

reinforced by Equation 3.10, which shows how R_r depends upon it.

In order to determine the quality of the experimental statistics, it is necessary to define two more quantities: the Signal to Background Ratio (SBR) and the relative error [73]. The SBR is the ratio of the number of true coincidence counts, R_t , to the number of random coincidence counts, R_r :

$$\begin{aligned} \frac{R_t}{R_r} &= \frac{nI\sigma^5\Delta E_a\Delta E_b\Delta\Omega_a\Delta\Omega_b\delta(E_0 - E_a - E_b - \epsilon_i)}{R_aR_b\Delta t_c} \\ &= \frac{nI\sigma^5\Delta E_a\Delta E_b\Delta\Omega_a\Delta\Omega_b\delta(E_0 - E_a - E_b - \epsilon_i)}{(nI)^2\left(\frac{\sigma^2}{d\Omega_a dE_a}\right)\left(\frac{\sigma^2}{d\Omega_b dE_b}\right)\Delta\Omega_a\Delta E_a\Delta\Omega_b\Delta E_b\Delta t_c}. \end{aligned} \quad (3.13)$$

This, in turn, can be simplified as the numerator is a convolution of $\Delta E_a\Delta E_b\delta(E_0 - E_a - E_b - \epsilon_i)$ while the denominator is $\Delta E_a\Delta E_b$. Thus:

$$SBR = \frac{R_t}{R_r} = \frac{\sigma^5}{nI(\sigma^2)_a(\sigma^2)_b\Delta t_c} \times \frac{\Delta E_s}{\Delta E_l}, \quad (3.14)$$

where ΔE_s is the smaller of ΔE_a and ΔE_b , and ΔE_l is the larger of the two.

By reducing nI and Δt_c , or letting $\Delta E_s = \Delta E_l$, in Equation 3.14, it is possible to improve the experimental statistics. The simplest way to do so is to decrease the target density, n , or incident current, I , although doing so has a negative impact on the number of true coincidence counts, as seen in Equation 3.9 and, in turn, the relative error.

It is now possible to arrive at the number of true coincidence counts in the signal window, in terms of experimental parameters:

$$\begin{aligned} N_t &= R_t T \\ &= nI\sigma^5\Delta E_a\Delta E_b\Delta\Omega_a\Delta\Omega_b\delta(E_0 - E_a - E_b - \epsilon_i)T \\ &= nIA_t T, \end{aligned} \quad (3.15)$$

where T is the period of time over which the experimental data is collected and $A_t = \sigma^5\Delta E_a\Delta E_b\Delta\Omega_a\Delta\Omega_b\delta(E_0 - E_a - E_b - \epsilon_i)$.

The standard deviation for the revised number of true coincidence counts is given by:

$$\sigma_t = \sqrt{N_t + \frac{N_b(r+1)}{r^2}}, \quad (3.16)$$

CHAPTER 3. EXPERIMENTAL APPARATUS AND TECHNIQUES

which was obtained by substituting Equation 3.6 into Equation 3.8.

The total number of random coincidence counts in the background window can likewise be arrived at in terms of experimental parameters:

$$\begin{aligned}
 N_b &= rR_rT \\
 &= rR_aR_b\Delta t_cT \\
 &= r(nI)^2(\sigma^2)_a(\sigma^2)_b\Delta E_a\Delta E_b\Delta\Omega_a\Delta\Omega_b\Delta t_cT \\
 &= r(nI)^2A_b\Delta t_cT,
 \end{aligned} \tag{3.17}$$

where we now set $A_b = (\sigma^2)_a(\sigma^2)_b\Delta E_a\Delta E_b\Delta\Omega_a\Delta\Omega_b$ for the sake of simplicity.

By combining the number of true coincidence counts with the standard deviation of the true coincidence counts (Equations 3.15 and 3.16 respectively), we arrive at the relative error:

$$\begin{aligned}
 \frac{\sigma_t}{N_t} &= \pm \frac{\sqrt{N_c + \frac{N_b(r+1)}{r^2}}}{nIA_tT} \\
 &= \pm \frac{1}{A_t} \frac{1}{\sqrt{T}} \sqrt{\frac{A_t}{nI} + \frac{A_b\Delta t_c(r+1)}{r}}.
 \end{aligned} \tag{3.18}$$

Substituting A_t and A_b back into Equation 3.18 we find,

$$\frac{\sigma_t}{N_t} = \pm \frac{1}{\sqrt{(\Delta\Omega_a\Delta\Omega_b)}} \frac{1}{\Delta E_s} \frac{1}{\sqrt{T}} \sqrt{\frac{1}{nI\sigma^5} \frac{(\sigma^2)_a(\sigma^2)_b}{(\sigma^5)^2} \frac{\Delta E_a\Delta E_b}{(\Delta E_s)^2} \frac{(r+1)}{r}} \Delta t_c. \tag{3.19}$$

Furthermore, by setting $\Delta E_a = \Delta E_b = \Delta E$, Equation 3.19 can be further simplified to:

$$\frac{\sigma_t}{N_t} = \pm \frac{1}{\sqrt{(\Delta\Omega_a\Delta\Omega_b)}} \frac{1}{\Delta E} \frac{1}{\sqrt{T}} \sqrt{\frac{1}{nI\sigma^5} \frac{(\sigma^2)_a(\sigma^2)_b}{(\sigma^5)^2} \frac{(r+1)}{r}} \Delta t_c. \tag{3.20}$$

Thus, from the above equation (Equation 3.20), it is clear that the relative error can be reduced by collecting the data over a larger period, T , or by increasing the target density, n , the incident electron current, I , the energy resolution, ΔE , or the angular resolutions, $\Delta\Omega_n$. However, by doubling the experimental counting time, the relative error will only be reduced by a factor of $\sqrt{2} = 1.4$, due to the square root in Equation 3.20. Additionally, increasing the target density or incident electron current will lead to a decrease in the SBR (Equation 3.14). Therefore the most effective method to decrease the relative error is to increase the energy and angular resolutions. Thus optimising a coincidence experiment

requires exercising judgement on a number of competing factors.

3.2.2 Energy Resolution

The combined energy resolution of the electron gun and both analysers, ΔE_c , can be expressed as [66]:

$$\Delta E_c^2 = \Delta E_0^2 + \left(\frac{1}{\Delta E_a^2} + \frac{1}{\Delta E_b^2} \right)^{-1}, \quad (3.21)$$

providing that the energy resolutions of the electron gun and analysers have a Gaussian profile.

It is not possible to measure ΔE_c experimentally, and yet it is used for calculating the cross sections from the coincidence count rates or deconvolving data [90]. An indication of ΔE_c can however be gleaned from the binding energy resolution, ΔE_{BE} [90, 91], given by:

$$\Delta E_{BE} = \sqrt{(\Delta E_0^2 + \Delta E_a^2 + \Delta E_b^2)}. \quad (3.22)$$

It has been shown both experimentally [90] and theoretically [91] that the effective coincidence energy resolution is not the same as the resolution obtained from a binding energy spectrum, ΔE_{BE} , however, it is still an important quantity as it represents the ability of the (e,2e) spectrometer to resolve close-lying valence electronic states. Note at this time that the (e,2e) technique does not resolve these states to the same degree of accuracy attainable by other spectroscopic techniques [2]. It is for this reason that photoelectron spectroscopic information plays such an important role in assigning orbitals to collected (e,2e) binding energy data.

3.2.3 Chamber Alignment

For all intents and purposes, the interaction region of the scattering chamber is often considered to be an infinitely well resolved point in space. In actual fact, the interaction region occupies a finite area as defined by the overlap of the molecular target beam, the electron beam, and the viewing volumes of the ejected and scattered electron analysers. A schematic diagram of the interaction region illustrating these features can be seen in Figure 3.11.

If the size of the interaction region were to change due to the analysers moving through the scattering plane, then the number of true coincidence counts measured would be inaccurate. In particular, with respect to the current mea-

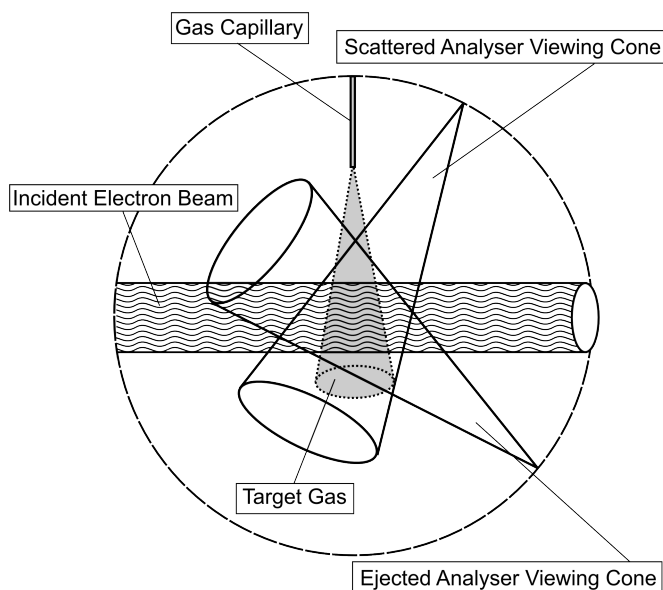


Figure 3.11: A schematic diagram of the scattering region as seen from above.

surements, the number of true coincidences as a function of θ_b , for a given θ_a , would be distorted and not represent a true measure of the TDCS for a given ionisation process. In order to eliminate this effect, so that the true coincidence count rate is dependent only on the physical properties of the ionisation process, accurate alignment of all the (e,2e) spectroscopic components must be performed.

The interaction region is centred in the chamber, 2-3mm above the stainless steel capillary that extends from the molecular oven discussed in Section 3.1.5. Alignment of the various (e,2e) spectroscopy components is achieved by temporarily slipping a glass capillary, that bears two marks, over the oven's stainless steel capillary. One of these marks represents where the stainless steel capillary ends and is one colour, while the other mark is a different colour and represents the interaction region location.

The electron gun is aligned to the interaction region through the use of a surveyor's telescope, which is focused through the two apertures within the electron gun (see Figure 3.4) at the visual reference on the glass capillary. Apart from simply ensuring that the gun is correctly aligned with the interaction region, this method also ensures that the apertures within the electron gun are correctly aligned. If the apertures are in any way misaligned, visually the "barrel" of the electron gun will appear to be of an elliptical shape rather than the circular

shape that is expected.

On the other hand, the analysers have a number of alignment options available, due to their relatively large viewing volumes. In addition to using the surveyor's telescope, it is also possible to visually align the analysers, without its aid, by using an alignment hole drilled through the relevant hemisphere which is aligned with the analyser's electron optics (see Figure 3.5). A laser may then also be directed through that alignment hole in order to provide visual feedback on the state of the system alignment. The preferred method, however, is to make use of alignment rods which are threaded through the alignment hole and relevant electron optics lens stack. The alignment rods are preferred as the analysers can be rotated while the rods remain in place, providing instant visual feedback on the quality of the alignment of the analysers at a number of different angles.

3.3 Calibration

It is important to regularly calibrate the (e,2e) spectrometer to ensure its consistent and reliable operation, as well as minimising false or misleading data that can arise. For this particular (e,2e) spectrometer, it is necessary to calibrate the energy of the electron gun and analysers, as well as their actual scattered and ejected angles. Furthermore, it is advisable to run additional checks on well known cross sections and then compare the current results with those previous results to ensure the (e,2e) spectrometer is operating in a self-consistent fashion.

3.3.1 Energy Calibration

The (e,2e) process is based upon the principles behind the conservation of energy and if valid results are sought, then an accurate knowledge of the incident and outgoing electron energies is required. In order to maximise the number of true coincidence counts, the experimental energy offsets must be accurately determined in order to counteract the effects of patchfields and contact potentials that may occur within the scattering chamber. In order to determine the energy offset of the scattered analyser, the Auger process is utilised.

The Auger process is when an electron within the inner shell of an atom is ionised, allowing an electron in a higher energy state to drop into a lower energy state. When this occurs, the energy released is sufficient to eject a second "Auger" electron from the atom. This process is energy independent from the initial incident electron and provides a unique spectrum for every element. The Auger process is initiated with argon by an incident electron with an energy in

CHAPTER 3. EXPERIMENTAL APPARATUS AND TECHNIQUES

the region of 600eV, which interacts with an electron in the inner $2p$ shell. The resulting Auger lines are quite distinctive, the principal amongst them being the $L_{2,3}-M_{2,3}M_{2,3}$ lines, which lie in the energy range of approximately 200eV - 208eV [92].

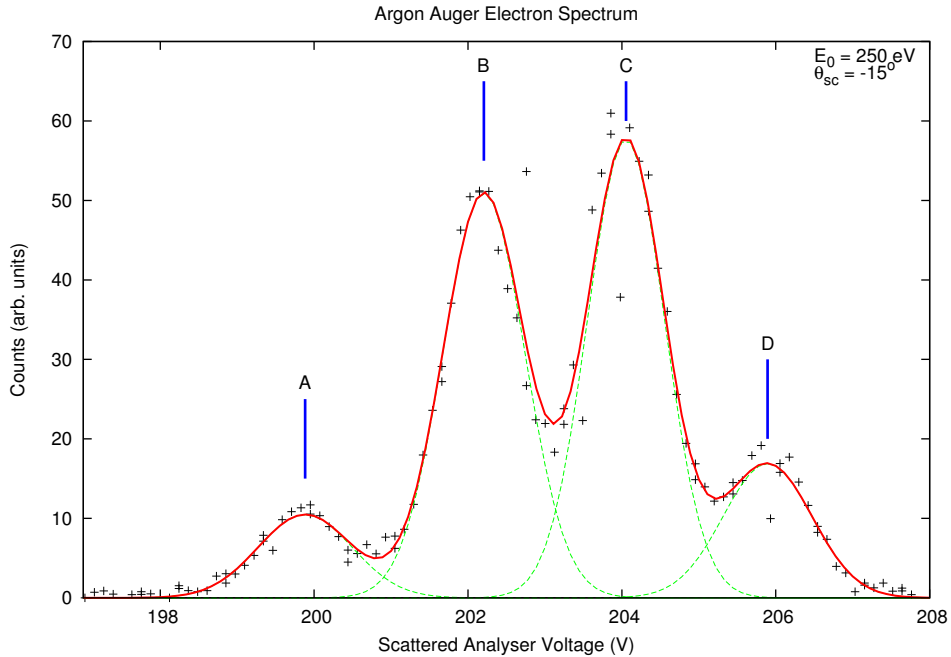


Figure 3.12: The primary Auger lines of argon, measured by the scattered electron analyser, and fitted to a number of Gaussian peaks. This is compared to the accepted literature peak locations [93] in order to correctly calculate the scattered electron energy offset. The Auger line assignments are: A) $L_3M_{2,3}M_{2,3}(^1S_0)$ (201.09eV), B) $L_3M_{2,3}M_{2,3}(^1D_2)$ (203.47eV), C) $L_3M_{2,3}M_{2,3}(^3P_{0,1,2})$ (205.21eV), and D) $L_2M_{2,3}M_{2,3}(^3P_{0,1,2})$ (207.23eV).

Thus by scanning the scattered analyser over the 200eV - 208eV range, and comparing the measured principal Auger line locations to the accepted literature values, the energy offset can be calculated [93]. However it is not possible to resolve all the possible peaks due to the energy resolution of the analyser, which does introduce a small uncertainty in this calibration process. It is worth noting at this point that the ejected analyser can also be calibrated in the same manner as outlined above.

In order to determine the energy offset of the incident electron, one of two methods is typically utilised. The first method required that the energy offset of either analyser has already been accurately determined, but once it has it becomes a trivial task to calibrate the incident beam energy. In this case the analyser is set to a specific energy for the elastic differential cross section, while the incident electron energy is scanned across an expected energy range. This

3.3. CALIBRATION

process continues until the energy with the maximum number of counts is determined and from that the energy offset can be extracted. This process can also be used as an alternative method to determine the energy offset of either analyser, but only if the incident electron offset is previously known from a different procedure.

The other method in which the incident electron energy offset can be determined, requires that the energy offsets for both analysers are known. By maximising the number of true coincidence counts detected via the coincidence method on a well known orbital energy, the energy beam offset can be defined. For this particular apparatus, the preferred choice is the Helium 1s shell, with a binding energy of 24.6eV [25]. An example of a result from this process, using helium, can be seen in Figure 3.13.

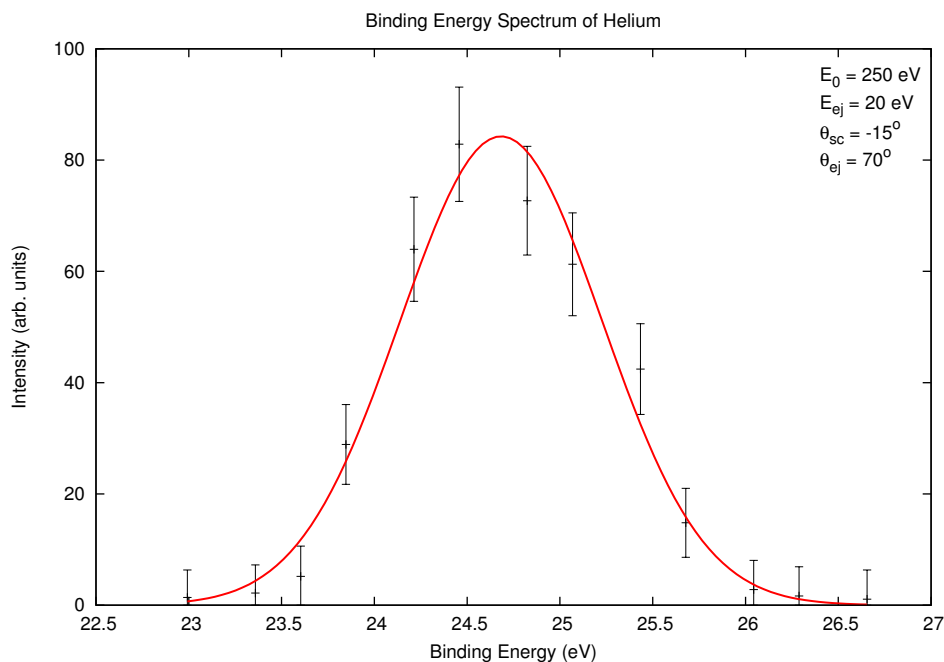


Figure 3.13: A binding energy spectrum for the helium 1s orbital. This peak in particular is important, as it can also be used to define the binding energy resolution, ΔE_{BE} , of an $(e,2e)$ spectrometer. In this particular example case, the binding energy resolution obtained was $\Delta E_{BE} = 1.5 \text{ eV}$ Full Width Half Maximum (FWHM).

3.3.2 Angular Calibration

It is extremely important to correctly calibrate the scattered and ejected electron angles of the $(e,2e)$ spectrometer, as a mechanical offset that can be measured in the TDCS spectrum will distort the underlying physics being studied. As such, a complete understanding of these physical effects will lead to a better

CHAPTER 3. EXPERIMENTAL APPARATUS AND TECHNIQUES

understanding of the collision process, so it is essential to correctly perform an angular calibration. This calibration is typically performed using either elastic Differential Cross Sections (DCS) or Double Differential Cross Sections (DDCS), on scattering systems that have particular features that make them optimal for calculating any angular offsets. It is, however, impractical to calibrate the analysers in the same manner, due to the mechanical limitations imposed by the various components within the spectrometer.

In order to calibrate the ejected electron analyser, the argon elastic DCS is measured at energies of 60eV and 100eV. Argon is used for this due to its rather distinct deep angular dependent minima that occur. At 60eV a single minimum occurs at 64° and at 100eV two minima occur at 58° and 123°. Another reason that argon in particular is used is that the angular dependent minima are nearly all capable of being accessed in the range of the ejected analyser (though it is worth noting that the current setup of the spectrometer makes it impossible to measure the minimum that occurs at 123°).

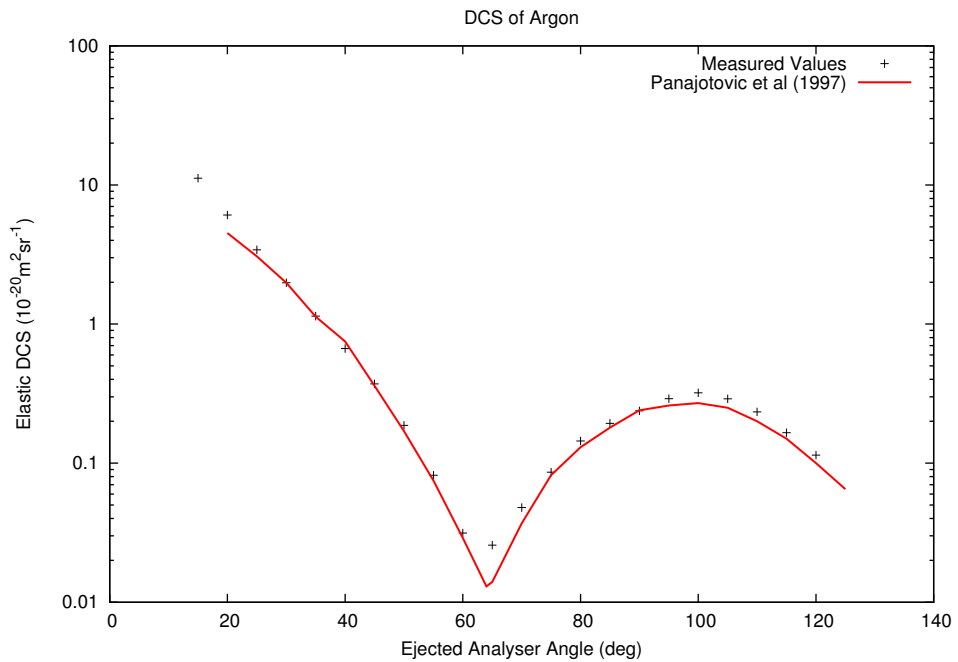


Figure 3.14: Elastic DCS of argon at 60 eV, typically used for the angular calibration of the ejected analyser. Note: the present measured values were normalised to Panajotovic *et al* [94] at 30°.

Once measured, the results of the elastic DCS are compared to the accepted literature values, as measured by Panajotovic *et al.* [94]. By doing so, it is possible to get an accuracy on the ejected electron scattering angle in the order of $\pm 1^\circ$. Figure 3.14 is an example of a measured 60eV elastic DCS of argon

3.3. CALIBRATION

compared to the results of Panajotovic *et al.*. The minor visual discrepancy between the measured results and the results of Panajotovic *et al.*, in Figure 3.14, is due to the current angular resolution being inferior to that of Panajotovic *et al.*.

Unlike the ejected analyser, the scattered electron analyser usually only moves through the rather limited range of $\pm 15^\circ$, although a much higher level of accuracy is now required due to the sensitivity of the TDCS on θ_a (see later). An accuracy of $\pm 0.5^\circ$ is achievable by measuring the symmetry of the DDCS around 0° , an example of which, using helium as a target, can be seen in Figure 3.15. The advantage of using this method of angular calibration, over any other, is the fact that it is gas independent, allowing for regular calibration to be performed without “switching” our target gases. It should be noted here, that after angular calibration has been performed, the electron gun deflectors settings are not modified.

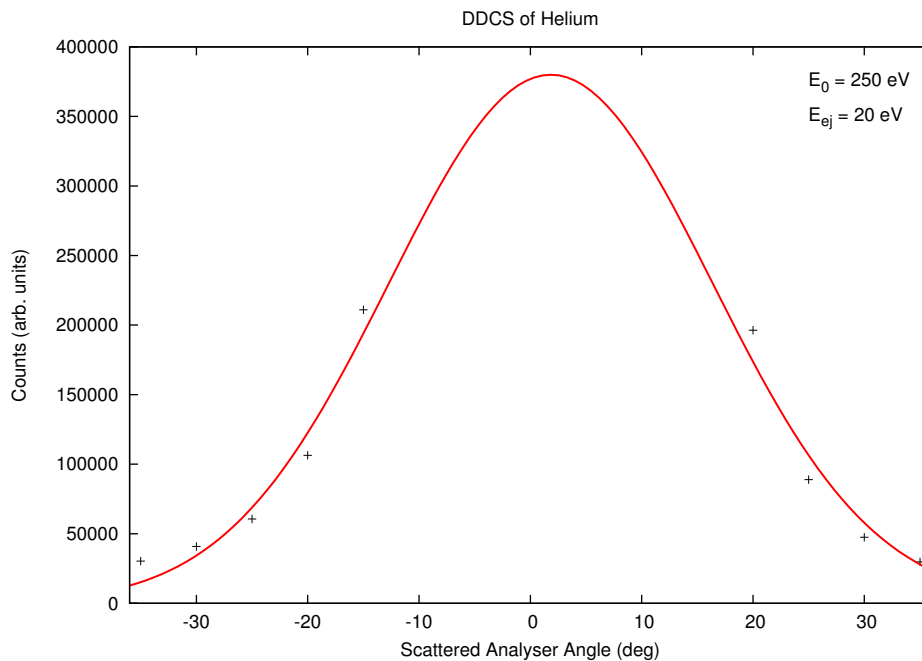


Figure 3.15: *The experimentally measured DDCS using the scattered electron analyser, performed symmetrically around a nominal 0° on helium, with a fitted Gaussian also shown.*

3.3.3 (e,2e) Spectrometer Self-Consistency Checks

As the present (e,2e) spectrometer is expected to collect experimental results over an extended period of time, its reliability must be ensured. In order to check the reliability of the (e,2e) spectrometer, two consistency checks can be

CHAPTER 3. EXPERIMENTAL APPARATUS AND TECHNIQUES

performed: a DDCS measurement and a TDCS measurement. In both cases, the measured result is compared to well known cross sections measured, or calculated, by independent third parties.

The first consistency check ensures that the analysers are not misaligned, and is performed by measuring the DDCS of helium with 200eV incident electrons and 10eV or 50eV ejected electrons. This particular DDCS is highly sensitive to the volume overlap of the incident electron beam, the molecular gas beam and the two viewing cones of the analysers [66] (see Figure 3.11 for a schematic view). As the analysers are rotated through various angles, it is expected that the measured and known results will remain consistent, as any observed change suggests that the volume overlap has changed which, in turn, suggests a misalignment.

The other consistency check that is performed is designed to ensure that the (e,2e) spectrometer is working optimally. This is achieved by measuring the TDCS of helium or argon under the same kinematic conditions as that for the less studied or never before studied target of interest. The TDCS of He, for instance, is then compared to the corresponding results measured by Colyer [15], a Distorted Wave Born Approximation (DWBA, see Section 2.5.2) result calculated with the same kinematic conditions by McCarthy *et al.* [95], and a Convergent Close-Coupling (CCC) calculation by Bray *et al.* [96, 97]. As you can see from Figure 3.16, there is quite good agreement between the present experimental results, previous experimental results and calculated theories, suggesting that the present (e,2e) spectrometer can be operated in a reliable and consistent manner.

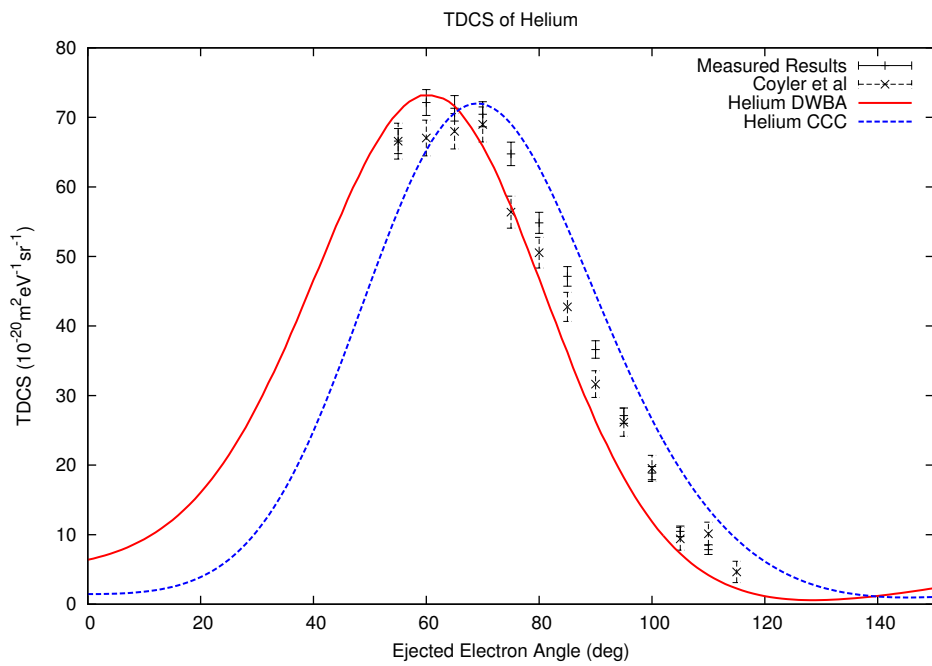


Figure 3.16: The measured TDCS of helium for 250 eV incident electrons, 20 eV ejected electrons, with the scattered electrons detected at -15° , compared to the experimental results found by Colyer [15], and with the DWBA calculations of McCarthy et al. [95] and the CCC calculations of Bray [96], all being conducted under the same kinematic conditions. The angular uncertainty of the experimental results is expected to be up to $\pm 2.5^\circ$, and as such does not encompass the offsets seen in the CCC and DWBA results.